(Preprint)

A Comparative study of the tensile properties of compression molded and 3D printed PLA specimens in dry and water saturated conditions

Vikas Chandran[1], Jordan Kalman[2], Kazem Fayazbakhsh[3] and Habiba Bougherara[4]

[1,2,3]Department of Aerospace Engineering, Ryerson University, 350 Victoria Street, Toronto, ON, Canada, [4]Department of Mechanical and Industrial Engineering, 350 Victoria Street, Toronto, ON, Canada

(Received 000 0, 2020; Revised 000 0, 2020; Accepted 000 0, 2020)

Keywords: Fused filament fabrication (FFF); Compression molding; Mechanical properties; Water absorption; Failure

Correspondence to: Habiba Bougherara / Habiba.bougherara@ryerson.ca **DOI:** https://doi.org/10.1007/s12206-021-0415-5

Abstract This research work presents a comparative study of the tensile properties of polylactic acid (PLA) specimens per ASTM D638-14 fabricated by compression molding and 3D printing. PLA pellets from one batch are used in compression molding and filament extrusion for 3D printing. The compression molding process parameters are optimized to obtain an upper limit for mechanical properties of PLA specimens. Design of Experiments (DoE) is used to evaluate the effect of processing temperature, pressure, and dwell time on the tensile properties of the specimens. The optimum compression molding trial resulted in slightly higher modulus for tensile specimens compared to 3D printing (3.33 GPa versus 3.22 GPa), while the average tensile strength was almost identical (59.9 MPa). Water absorption test is performed to evaluate moisture absorption of tensile specimens and compare their tensile properties in water saturated condition to the properties of dry specimens. 3D printed specimens showed a significant degradation of their tensile strength and modulus in water saturated condition by 28.4% and 7.2%, respectively. On the other hand, the tensile strength of the optimum compression molded specimens was decreased by only 12.0%, while there was an increase of 14.1% in tensile modulus.

1. Introduction

The fabrication of highly customized polymer parts with minimal cost is a huge challenge being encountered in the manufacturing sector regardless of the application. Therefore, while choosing the best production methods for polymer components, factors such as design, precision, material, cost, and volume of production should be weighed. For instance, compression molding (CM) is a viable choice to fabricate medium to large size simple flat products, while fabrication of structures with complex geometric features intended for specific applications requires a special production technology. Hence, if the product does not require unique features and complex design, CM may be a practical choice. Three-dimensional (3D) printing on the other hand, is a promising technology that offers many benefits, including the ability to fabricate functional components with customized features [1-3]. This manufacturing technology can produce polymer products with complex geometries by sequential layering of materials using computer aided designed 3D models without the need of a physical mold [4]. There is an emerging consensus of adapting 3D printing as an alternative to conventional methods in the manufacturing sector because it has brought automation and has surpassed traditional manufacturing techniques in terms of cost, efficiency, and design flexibility. Among various 3D printing methods, fused filament fabrication (FFF) is a widely employed technique for printing thermoplastic components on account of its simplicity, low cost, and minimal wastage of materials [5]. It produces a 3D geometry through the successive deposition of molten thermoplastic filament such as, acrylonitrile butadiene styrene (ABS) [6] and polylactic acid (PLA) [7, 8] in a layer-by-layer fashion [7]. FFF has edge over other printing techniques in manufacturing small series of finished parts at relatively reduced cost, which has encouraged researchers and engineers to employ this technology for manufacturing prototypes or products utilizing thermoplastic polymers.

Among thermoplastic polymers, PLA is a widely used biodegradable polymer due to its low cost, good mechanical strength, and high dimensional accuracy. Biopolymer PLA is considered as a potential alternative to petroleum-based plastics and a crucial component in biomedical, structural engineering applications, and can perform efficiently in cryogenic environments [9]. Further, PLA has the advantage of easy processability both in conventional techniques (extrusion, compression molding, and injection molding) and emerging technology like 3D printing. The properties of the PLA parts can be tailored by changing the molecular weight of polymer and different crystal structures and extent of crystallinity can be created by varying the thermal profile

of the material [10, 11]. Because of these attributes, scientific explorations on PLA in 3D printing technology have emerged significantly in both volume and scale [10-12]. The prior published literature revealed the dependence of the mechanical performance of PLA 3D printed parts on processing parameters, such as build orientation, layer thickness, raster angle, and printing speed [13, 14].

The optimum selection of the 3D printing process parameters can result in final parts with adequate mechanical performance to widen their application from solely prototyping. Few researchers used the same grade of raw material in traditional manufacturing techniques and for extruding filaments as feedstock for 3D printing [15-20]. This enabled a true comparison between 3D printed and injection molded [15-19] or compression molded parts [20]. Weng et al. [15] used neat ABS and ABS reinforced with organic montmorillonite (OMMT) and found 45% and 37% reduction in tensile strength and modulus, respectively, for ABS 3D printed specimens compared to injection molded ones. Miller et al. [16] witnessed 3D printed specimens from polycarbonate urethane (PCU) with significantly larger failure strains in tension compared to injection molded ones, despites very similar tensile strength values. Kaynak and Varsavas [17] utilized PLA and its mix with TPU and found similar tensile strength between 3D printed and injection molded specimens, while the tensile modulus of 3D printed specimens were up to 13% higher. Ecker et al. [18] and Lay et al. [19] investigated the impact of water absorption on mechanical properties of 3D printed and injection molded specimens. They found higher water uptake for 3D printed specimens and a large reduction in their tensile properties compared to injection molded specimens. While previous studies focused on injection molding, Carneiro et al. [20] investigated compression molding as the baseline and observed around 20% reduction in the mechanical properties of the polypropylene (PP) 3D printed samples compared to the compression mold ones. They did not use optimum 3D printing process parameters and did not investigate water absorption behaviour of the specimens.

This paper provides a comparative study of the tensile properties of compression molded and 3D printed PLA specimens per ASTM D638-14. PLA pellets from one batch are used in the compression molding and filament extrusion for 3D printing. First, compression molding parameters, namely processing temperature, pressure, and dwell time, are optimized using Design of Experiments (DoE) to find the upper limit of tensile properties for PLA specimens. Then, Water absorption test per ASTM D5229-14e1 is performed to evaluate moisture absorption for optimum compression molded and 3D printed specimens. Finally, tensile properties of CM and 3D printed specimens in dry and water saturated conditions are compared. Digital micrographs of the fracture surfaces are discussed, and the paper wraps up with conclusions and directions for future research studies.

2. Materials and methods

2.1 Materials

PLA pellets (Ingeo 4043D, NatureWorks LLC, Blair, Nebraska) from one batch were used in this study [21]. Differential Scanning Calorimetry (DSC) was performed to find its glass transition and melt temperatures following ASTM D3418-15 [22]. Samples of 6-10 mg were extracted from the PLA pellets and were used in the DSC Q100 machine from TA Instruments. To remove thermal history of the material, first, a heat run was performed in dynamic mode from room temperature to 200 °C at a rate of 10 °C/min. Then, samples were cooled down to ambient temperature at 5 °C/min and were kept there isothermally for 3 min. The second heat run in dynamic mode was performed at a rate of 5 °C/min from room temperature to 200 °C to capture glass transition and melt temperatures. The heat flow cures versus the temperature scan are shown in Fig. 1 indicating a glass transition temperature of 58.7 ˚C and 150.3 ˚C melting temperature for the PLA pellets. These values agree with the temperature ranges provided by the material supplier of 55-60 °C and 145-160 °C for glass transition and melt temperatures, respectively [21].

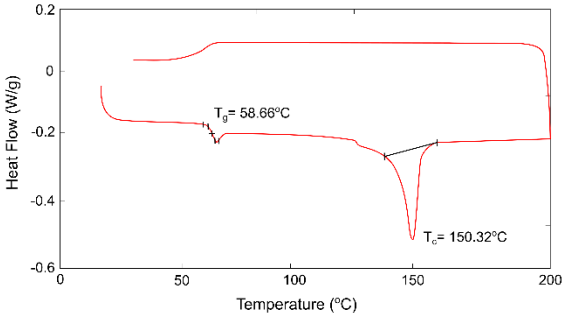

Fig. 1. The DSC thermograms of the PLA pellets.

2.2 Specimen manufacturing

2.2.1 Compression molding

PLA specimens were manufactured using a hydraulic press (Carver Auto Series) with two heated platens of 15 × 15 in. dimensions and that could provide a maximum clamping force of 30 tons. PLA pellets were put on in-house low carbon 12 × 12 in. steel mold having a total of 11 specimen cavities per ASTM D638-14 type I. Each specimen cavity in the mold was filled with 20g of PLA pellets and gradually heated from room temperature to desired processing parameters, i.e. temperature, pressure, dwell time, and cooling time. Fig. 2 shows the general depiction of fabrication setup, CAD model of the mold, physical mold filled with PLA pellets, compression molding machine, and the fabricated PLA

specimens. It should be noted that only to ensure easy removal of tensile specimens and guard them from being damaged, small metal tabs were added on either side of the cavity.

To optimize the compression molding processing parameters, Taguchi's Design of Experiments (DoE) trials were utilized. The minimum number of experiments to be conducted based on Taguchi's DoE was calculated using:

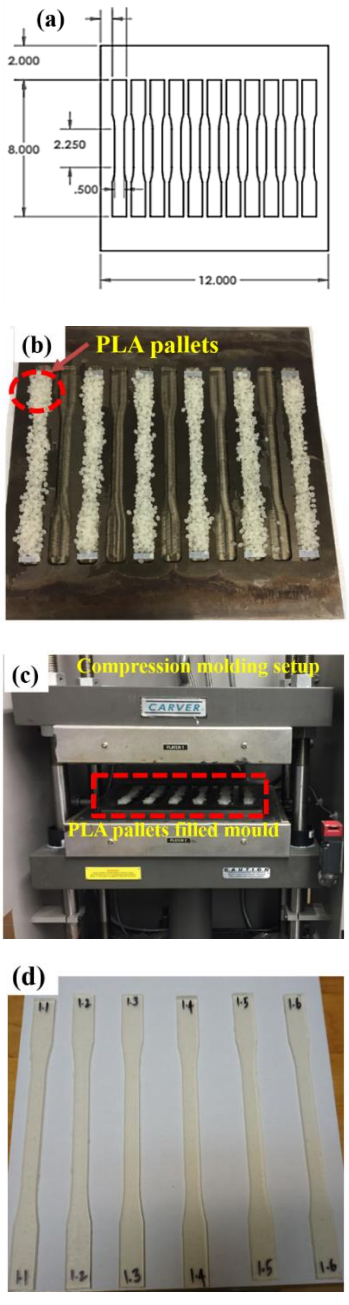

Fig. 2. Fabrication setup: (a) CAD model of the mold (in.); (b) physical mold filled with metal tabs and filled with PLA pellets; (c) compression molding machine; and (d) PLA specimens fabricated by CM.

$$N_{Taguch} = 1 + \sum_{i=1}^{NV} (L_i - 1) \quad (1)$$

Where NV is the number of variables and L_i is the number of levels identified for each variable. For this study, temperature, pressure, and dwell time are considered as variables in the compression molding process (NV=3) and three levels are considered for each variable (L_i = 3). Using Eq. (1), at least seven experiments need to be performed, but due to the balancing property of Taguchi's orthogonal array, number of experiments must be a multiple of three. Thus, a total of nine experimental trials are determined as shown in Table 1. The cooling temperature of 30 °C for all specimens have been achieved with the automated cooling cycle assisted by the compression molding machine and over the same period (10 min).

As mentioned before, six (6) specimen cavities were used for manufacturing tensile specimens for each trial bringing the total compression-molded specimens to 54.

2.2.2 Filament extrusion and specimen 3D printing

The same batch of PLA pellets used in the compression molding process was utilized in a single screw extruder to manufacture filaments for 3D printing. A dehydration process on the pellets was performed at 60 °C for 4 hours to reduce the moisture content of the pellets

Table 1. Test plan for compression molding process per Taguchi's technique.

Experiment. (or Trial No.)	Temp. (°C)	Pressure (MPa)	Dwell Time (min)
1	150	2	10
2	150	2.5	20
3	150	3	30
4	160	2	20
5	160	2.5	30
6	160	3	10
7	170	2	30
8	170	2.5	10
9	170	3	20

to below 250 ppm. The pellets were then fed into a single screw filament extruder (FilaFab, D3D Innovations Limited, Bristol, UK) connected to a spool winder. Throughout the process, the filament diameter was consistently monitored using a laser micrometer with ±2 μm accuracy. The extrusion parameters including the die temperature, screw speed, die diameter, and the winder speed were properly adjusted to achieve a 1.75 ± 0.05 mm filament diameter consistently, comparable

to commercial filaments used in 3D printing. The extrusion temperature, screw speed, die diameter and winder speed were optimized in a previous study [23] and set to 210 °C, 25 rpm, 2 mm and 1 rpm, respectively.

A Prusa i3 MK2S 3D printer firmware version 3.1.0 was used to process the extruded PLA filaments and manufacture six tensile specimens in the flat orientation (XYZ) per ISO/ASTM 52921:2013(E) [24]. The 3D model of the specimen was created in SolidWorks and was transferred to Simplify3D version 4.1.2 to prepare G-codes for FFF 3D printing. Design and manufacturing process parameters for 3D printing were optimized in a previous study [25] and were used here to manufacture the specimens (Table 2).

The raster angle was selected as 0° since tensile strength and modulus along the extrudates represent the highest values that can be achieved through the 3D printing process and can be used for comparison purposes with other manufacturing techniques, like compression molding. Tensile specimens per ASTM D638 type I have a thickness of 3.36 mm and consist of 24 layers each 0.14 mm thick and all in 0 deg orientation, $[0]_{24}$ stacking sequence. Fig. 3 shows 3D printed tensile specimens out of pure PLA.

Table 2. Manufacturing and design parameters for FFF 3D printing.

Design/Manufacturing Parameter	Value	Design/Manufacturing Parameter	Value
Build orientation	XYZ	Raster angle	0º
Filament diameter	1.75 mm	Nozzle diameter	0.4 mm
Layer height	0.14 mm	Nozzle temperature	215 °C
Bed temperature	60	Cooling	No fan cooling
Printing speed	2400 mm/min	Infill %	100%

2.3 Experimental testing

Tensile tests of compression molded and 3D printed PLA specimens were conducted following ASTM D638-14 standard [26]. An electromechanical testing machine from United testing systems Canada with a 10 kN (2248 lbf) load cell and an axial clip-on extensometer with a 25% strain limit were used. Width and thickness of all the specimens were measured using a caliper to the nearest 0.025 mm (0.001 in). Three measurements for width and thickness were made for each sample, and their average values were used in the calculations. The specimens were placed in the mechanical wedge action tensile grips of the testing machine and their long axis was aligned with the loading line of action. The grips were tightened evenly and firmly to prevent specimen slippage during testing without exerting excessive clamping force that might result in crushing the specimen ends. Temperature and humidity inside the testing room were monitored and controlled, and followed standard laboratory atmosphere of 23 ± 3 °C and 50 ± 10% relative humidity. A constant crosshead speed of 5 mm/min (0.2 in/min) was applied, and the load-extensive curve of the specimens until the moment of rupture. A total of 54 compression molded specimens per Table 1 were tested and compared to the six 3D printed specimens.

Water absorption tests were conducted following ASTM D5229-14e1. Per optimum compression molding trial found from tensile testing, a total of five compression molded specimens and five 3D printed specimens were manufactured and tested for water absorption. The specimens were dried in an oven at 50 ºC for 24 hours, and then placed in a container filled with distilled water and maintained at room temperature. After 2 hours of immersion, all the specimens weighed to the nearest 0.001 g, which were again placed in water and weighed after 24, 48, 72, 96, 120, 288, and 456 hours of immersion. Following immersion in water, the specimens were assessed in tension in standard laboratory atmosphere to ascertain the effects of water absorption on tensile properties. The fracture pattern of PLA specimens was obtained using digital microscope USB2-MICRO-250X with magnification of up to 250x.

3. Results and discussion

Tensile tests were carried out to examine the effect of processing parameters on tensile properties of compression molded and 3D printed PLA specimens. In addition, tensile testing after 456 hours of water immersion was performed to evaluate the impact of water absorption on tensile properties of the specimens.

3.1 Dry condition

It is crucial to determine which combination of processing temperature, pressure, and dwell time produces the best compression molded PLA specimen, so that a comparison could be made with 3D printed specimens. Fig. 4 presents a graphical comparison of tensile properties obtained from different trials of compression molded specimens.

Trial #8 exhibited the highest tensile strength value closely followed by trials #5, 2 and 6, while trial #7 showed the lowest strength. On the contrary, trial #5 demonstrated the highest tensile modulus, while trial #6 had the lowest tensile modulus.

The values of tensile strength, modulus, and failure strain are included in Table 3 along with their respective

Fig. 3. Six 3D printed specimens out of extruded filaments.

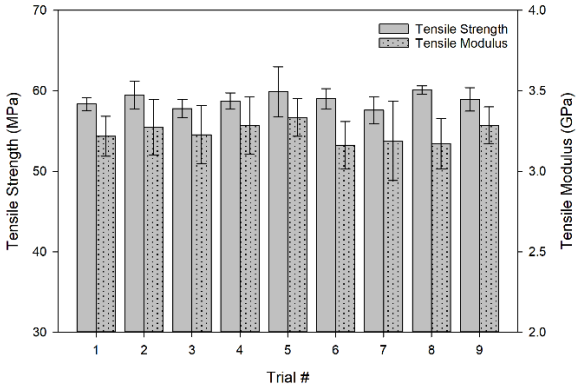

Fig. 4. Tensile strength and modulus from different compression molding trials.

Coefficient of Variation (CV). To find the optimum compression molding trial, weighted average property (WAP) was calculated by considering the tensile strength and tensile modulus of each trial as follows:

$$WAP = \frac{\sigma_U}{\max(\sigma_U)} \times 0.5 + \frac{E}{\max(E)} \times 0.5 \qquad (2)$$

Where σ_U is the mean tensile strength and E is the mean modulus of a respective trial, $\max(\sigma_U)$ is the maximum value of the mean tensile strength and $\max(E)$ is the maximum value of the mean modulus among all the compression molded trials.

Considering WAP values, Trial #5 was found to have the optimum process parameters among all the compression-molded trials. For various temperature conditions, the optimum processing pressure was found to be 2.5 MPa. The optimum processing temperature was 160 ˚C, which is about 10 ˚C more than the melting temperature of PLA (150.3 ˚C) obtained from the DSC test. With a processing temperature of 150 ˚C, it was observed that the PLA pellets did not melt completely, which formed voids in the specimens and made them brittle. On the other hand, at higher processing temperature (170 ˚C), the PLA pellets tend to vaporize. Since

Table 3. Tensile test results from the nine compression molding trials.

Trial #	Mean Strength (MPa)	CV (%)	Mean Modulus (GPa)	CV (%)	Mean Failure Strain (%)	CV (%)	WAP
1	58.4	1.4	3.22	3.9	1.99	2.9	0.968
2	59.5	2.9	3.27	5.3	2.15	5.0	0.986
3	57.8	2.0	3.23	5.6	1.99	6.3	0.965
4	58.7	1.7	3.28	5.5	2.09	4.1	0.981
5	59.9	5.2	3.33	3.5	2.11	3.5	0.998
6	59.0	2.1	3.16	4.6	2.10	3.9	0.965
7	57.6	2.9	3.19	7.8	2.04	2.6	0.958
8	60.1	0.8	3.17	4.8	2.22	2.3	0.976
9	59.0	2.5	3.29	3.4	2.02	5.4	0.983

under the given pressure the possibility of vapour escaping the system was unlikely, the number of voids was found relatively high. The processing parameters corresponding to trail #5 (temperature of 160 °C, pressure of 2.5 MPa, and dwell time of 30 min) were optimum and completely melted the PLA pellets with minimum void formation.

Tensile testing was repeated for six (6) 3D printed specimens and the following tensile properties were obtained: tensile strength (59.9 MPa, CV: 5.5%), modulus (3.22 GPa, CV: 3.8%), and failure strain (2.25%, CV: 7.9%). Fig. 5 represents the stress-strain curves of compression molded (trial #5) and 3D printed PLA specimens showing the maximum recorded tensile strength and failure strain. The average tensile modulus of optimum compression-molded specimens (3.33 GPa) was slightly higher compared to that of 3D printed specimens (3.22 GPa), while the average tensile strength was almost identical (59.9 MPa) and 3D printed specimens showed a higher failure strain (2.25% versus 2.11%). Unlike the work of Carneiro et al. [20], where they observed around 20 % reduction in the mechanical properties of 3D printed PP specimens compared to compression molded ones, the optimum

FFF process parameters used in this study resulted in similar tensile properties between the two manufacturing techniques. A Student's t-test is performed to compare tensile modulus and failure strain of compression-molded (train #5) and 3D printed specimens. It was found that there is not a statistically significant difference between tensile modulus (P = 0.143) and failure strain (P = 0.135) of the specimens. These results confirm that the optimum process parameters for 3D printing can manufacture specimens with tensile properties close to the ones from specimens manufactured using compression molding, a conventional manufacturing technique. The average tensile strength and modulus of the FFF 3D printed PLA parts are in line with those reported in the material technical data sheet for injection molded specimens by NatureWorks [21].

Fig. 6 shows the fracture surface of the compression molded (trial #5) and 3D printed specimens after tensile testing. The specimens fabricated by CM exhibited brittle failure (Fig. 6a) which occurred in the same plane (i.e., linear breakage). On the other hand, the 3D printed PLA specimens did not rupture in a single plane, instead it showed irregular breakage with zigzag form

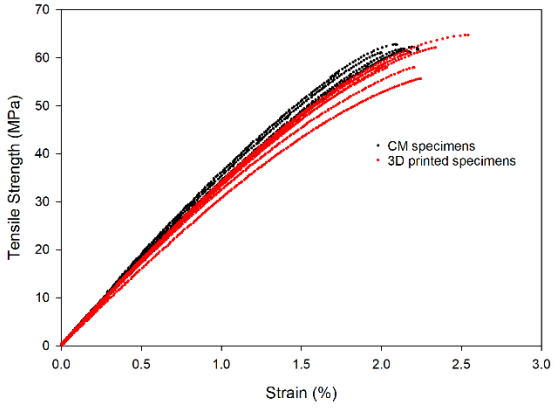

Fig. 5. Stress-strain curve for CM and 3D printed specimens.

or jagged line as shown in Fig. 6b. The cross section of the fractures surface exhibited loose structure with voids between the layers and distinct appearance of layers separation was visible. Most of the 3D printed specimens failed at a point close to the grips, which has been the common failure pattern for FFF 3D printed specimens [27], The reason for specimens being ruptured close to the grips area is attributed to the presence of stress concentration at fillet areas due to extrudates. The presence of gaps at the center of the specimens can also accumulate stress leading to premature failure [28-29]. In general, a uniformly distributed diffusion is required to minimize the infill gaps between the PLA extrudates and improve the bond strength. Thus, based on the pattern of the failure, it is stipulated that the weakest area might have generated at a point close to the grip during printing of the PLA specimens.

Fig. 7 shows the digital micrographs of the fracture surface of CM and 3D printed PLA specimens. The cross section of CM specimen (Fig. 7a) exhibited a homogenous and smooth brittle fracture texture with no apparent voids. This indicates that the optimum temperature and pressure created better bonding between the materials resulting into a dense structure. Conversely, 3D printed specimens comprised multiple layers and multiple voids between the layers can be observed (Fig. 7b). As FFF 3D printing is based on the layer by layer deposition of materials, air may have been trapped in the layers creating voids and consequently loosening the packing of layers. This led to a slightly lower tensile modulus of the 3D printed PLA specimens compared to CM specimens.

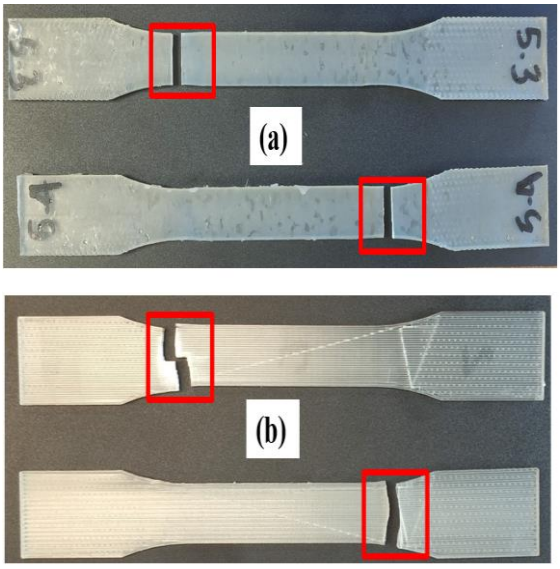

Fig. 6. Fracture pattern for tensile specimens (a) compression molded; and (b) 3D printed specimens.

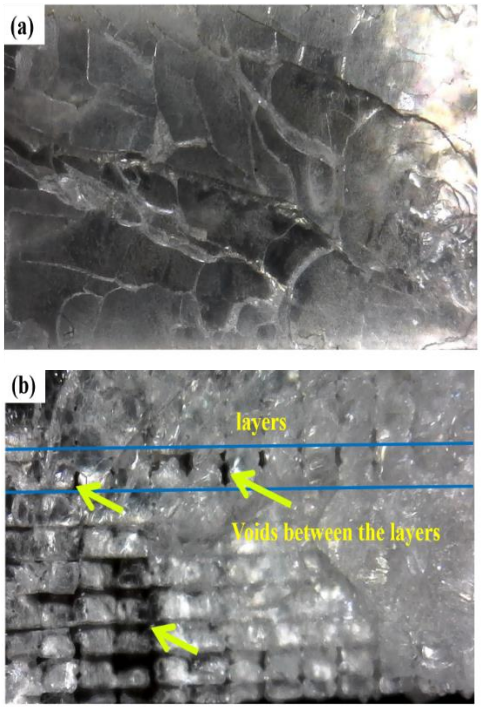

Fig. 7. Digital micrographs of the fracture surface of tensile specimens: (a) compression molded; and (b) 3D printed specimen.

3.2 Water saturated condition

Water absorption tests were carried out to evaluate the moisture absorption of the compression molded and 3D printed PLA specimens (five each). In addition, the tensile properties of the specimens in water saturated condition were compared to the properties of dry specimens. Fig. 8 shows the water absorption profiles for CM and 3D printed specimens for 456 hours. Specimens fabricated by both the manufacturing processes showed a linear initial rise in water absorption, eventually reaching a saturation. 3D printed specimens absorbed water at a higher rate than that of the CM samples and reached saturation with a larger amount of water absorption (weight percentage increase). For CM specimens, the weight percentage increase was found to be consistent and in a range between 0.78- and 0.88 %, while this was between 1.32- and 5.54 % for 3D printed specimens. The substantial water absorption in 3D printed specimens compared to CM specimens is attributed in part to the high porosities induced by the 3D printing process (Fig. 7b). It is worth noting that both water absorption profiles followed Fick's law, consisting of a sharp increase in water uptake for up to 100 hours, followed by a steady increase around 300 hrs., and then stabilization.

To obtain tensile properties of specimens in water saturated condition, experimental testing was performed for CM and 3D printed specimens. Fig. 9 shows tensile strength and modulus of all specimens in dry and water saturated conditions. It can be seen that dry specimens have higher tensile strength for both compression-molded and 3D printed specimens compared to water saturated specimens. Compared to compression molded specimens, it was observed that 3D printed ones exhibited more degradation in tensile strength after water absorption. 3D printed samples underwent a reduction in strength by about 28.4 % compared to 12.0 % for CM specimens. The immersion of CM specimens in water led to an improvement in the

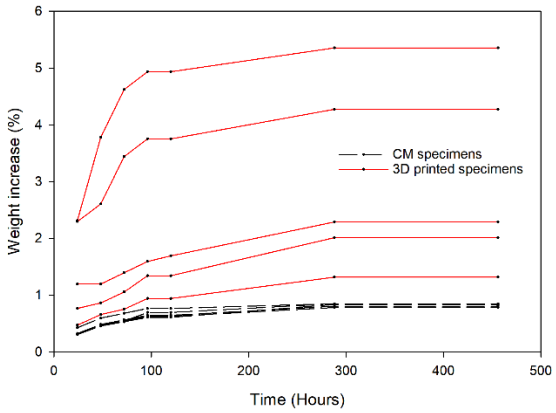

Fig. 8. Water absorption profiles of CM and 3D printed specimens.

tensile modulus as shown in Fig. 9. An increase in the tensile modulus of 14.1% on average was recorded for water saturated CM specimens, while the 3D specimens showed 7.2% decrease in the tensile modulus. The failure strain of CM specimens after immersion in water decreased significantly. The mean failure strain for CM specimens was decreased by 26.0 %, while there was a slight improvement of 4.7% for the case of 3D printed specimens.

The digital micrographs of the fracture surface of specimens in water saturated conditions are shown in Fig. 10. No significant change in the microstructure of CM specimens after water absorption was observed. However, for 3D printed specimens, voids between the layers were enlarged as indicated by the arrows in Fig. 10b. The presence of a larger number of voids increased the moisture absorption and led to their expansion. This

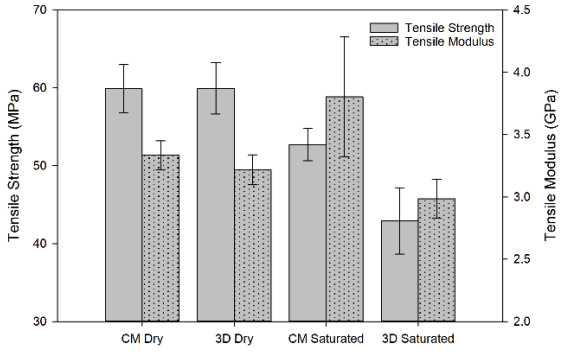

Fig. 9. Comparison of tensile properties of compression molding (CM) and

(3D) specimens in dry and water saturated conditions.

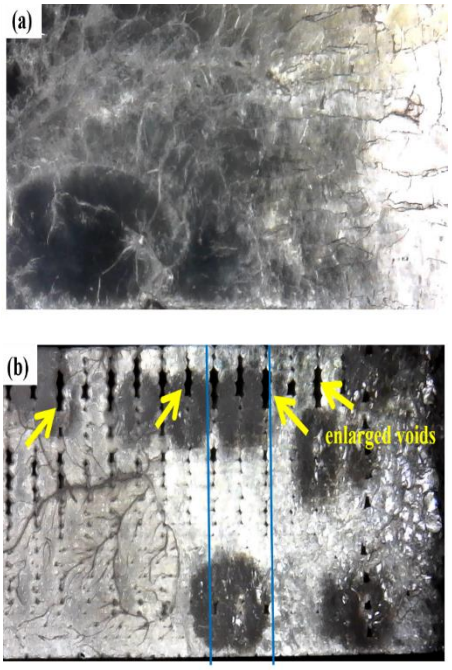

Fig. 10. Digital micrographs of the fracture surface of tensile specimens: (a) compression molded; and (b) 3D printed specimen.

might have led to delamination of layers causing the early failure of the specimens and contributed to the higher degradation in tensile properties of 3D printed specimens compared to compression molded ones.

4. Conclusions

This study presents a comparative performance analysis of the polylactic acid (PLA) tensile specimens fabricated by compression molding and 3D printing. The effects of the processing parameters on the tensile properties of compression molded specimens was analyzed using Design of Experiments and optimum manufacturing parameters have been determined. The mechanical performance of 3D printed specimens was compared to the performance of the specimens manufactured using optimum compression molding parameters. The average tensile strength of the specimens fabricated by both compression molding and 3D printing was identical (59.9 MPa), while compression molded specimen showed slightly higher modulus (3.33 GPa versus 3.22 GPa) and 3D printed specimens presented higher failure strain (2.25% versus 2.11%). These results indicate that the right 3D printing process parameters can result in specimens with tensile properties close to those of specimens manufactured using conventional manufacturing techniques. Water absorption test was performed to determine the moisture absorption of compression molded and 3D printed PLA specimens. In addition, their tensile properties in water saturated condition were compared with dry specimens. 3D printed specimens showed significantly larger amount of water absorption than CM specimens (3.92% versus 0.83% on average), leading to a substantial degradation of their tensile strength and modulus by 28.4% and 7.2%, respectively. The tensile strength of the compression molded specimens was decreased by 12.0%, while there was 14.1% increase in their tensile modulus. The presence of voids in 3D printed specimens increased the moisture absorption, which subsequently led to diminished mechanical performance.

For future work, other mechanical properties, e.g. in-plane and interlaminar shear, can be used to compare performance of compression molded and 3D printed specimens in both dry and water saturated conditions. In addition, polymer reinforced with short fibers can be investigated and these two manufacturing techniques can be compared in terms of the mechanical performance of the final products.

Acknowledgments

The authors would like to acknowledge Dr. Amirmohammad Rahimizadeh who performed DSC testing on PLA pellets for this study.

Nomenclature

WAP : Weighted average property
σ_U : Mean tensile strength
E : Mean modulus

References

[1] A. M. Peterson, Review of acrylonitrile butadiene styrene in fused filament fabrication: A plastics engineering-focused perspective, *Additive Manufacturing*, 27 (2019) 363-371.

[2] M. Harris, J. Potgieter, R. Archer, and K. M. Arif, Effect of material and process specific factors on the strength of printed parts in fused filament fabrication: A review of recent developments, *Materials*, 12 (10) (2019) 1664.

[3] G. D. Goh, Y. L. Yap, H. K. J. Tan, S. L. Sing, G. L. Goh, and W. Y. Yeong, Process–structure–properties in polymer additive manufacturing via material extrusion: A review, *Critical Reviews in Solid State and Materials Sciences*, 45 (2) (2020) 113-133.

[4] D. Zindania, and K. Kumar, An insight into additive manufacturing of fiber reinforced polymer composite, *International Journal of Lightweight Materials and Manufacture*, 2 (4) (2019) 267-278.

[5] T.D. Ngo, A. Kashani, G. Imbalzano, K.T. Nguyen, and D. Hui, Additive manufacturing (3D printing): A review of materials, methods, applications and challenges, *Composites Part B: Engineering*, 143 (2018) 172–196.

[6] W. Zhang, C. Cotton, J. Sun, D .Heider, B. Gu, B. Sun, and T. W. Chou, Interfacial bonding strength of short carbon fiber/acrylonitrile-butadiene styrene composites fabricated by fused deposition modeling, *Composites Part B: Engineering*, 137 (2018) 51–9.

[7] R. T. L. Ferreira, I. C. Amatte, T. A. Dutra, and D. Bürger, Experimental characterization and micrography of 3D printed PLA and PLA reinforced with short carbon fibers, *Composites Part B: Engineering*, 124 (2017) 88-100.

[8] N. Li, Y. Li, and S. Liu, Rapid prototyping of continuous carbon fiber reinforced polylactic acid composites by 3D printing, *Journal of Materials Processing Technology*, 238 (2016) 218–25.

[9] T. R. Tiersch, and W. T. Monroe, Three-dimensional printing with polylactic acid (PLA) thermoplastic offers new opportunities for cryobiology, *Cryobiology*, 73 (3) (2016) 396-398.

[10] R. A. Giordano, B. M. Wu, S. W. Borland, L. G. Cima, E. M. Sachs, and M. J. Cima, Mechanical properties of dense polylactic acid structures fabricated by three dimensional printing, *Journal of Biomaterials Science, Polymer Edition*, 8 (1) (1996) 63-75.

[11] H. Li, and M. A. Huneault, Effect of Nucleation and Plasticization on the Crystallization of Poly(lactic Acid), *Polymer*, 48 (23) (2007) 6855−6866.

[12] X. Wang, M. Jiang, Z. Zhou, J. Gou, and D. Hui, 3D printing of polymer matrix composites: A review and prospective, *Composites Part B: Engineering*, 110 (2017) 442–458.

[13] Y. Song, Y. Li, W. Song, K. Yee, K.Y. Lee, and V.L. Tagarielli, Measurements of the mechanical response of unidirectional 3D-printed PLA, *Materials & Design*, 123 (2017) 154–164.

[14] D. Popescu, A. Zapciu, C. Amza, F. Baciu, and R. Marinescu, FDM process parameters influence over the mechanical properties of polymer specimens: A review, *Polymer Testing*, 69 (2018) 157-166.

[15] Z. Weng, J. Wang, T. Senthil, and L. Wu, Mechanical and thermal properties of ABS/montmorillonite nanocomposites for fused deposition modeling 3D printing, *Materials & Design*, 102 (2016) 276-283.

[16] A. T. Miller, D. L. Safranski, K. E. Smith, D. G. Sycks, R. E. Guldberg, and K. Gall, Fatigue of injection molded and 3D printed polycarbonate urethane in solution, *Polymer*, 108 (2017) 121-134.

[17] C. Kaynak, and S. D. Varsavas, Performance comparison of the 3D-printed and injection-molded PLA and its elastomer blend and fiber composites, *Journal of Thermoplastic Composite Materials*, 32 (4) (2019) 1-20.

[18] J. V. Ecker, A. Haider, I. Burzic, A. Huber, G. Eder, and S. Hild, Mechanical properties and water absorption behaviour of PLA and PLA/wood composites prepared by 3D printing and injection moulding, *Rapid Prototyping Journal*, 25 (4) (2019) 672–678.

[19] M. Lay, N. L. N. Thajudin, Z. Ain Abdul Hamid , A. Rusli , M. K. Abdullah, and R. K. Shuib, Comparison of physical and mechanical properties of PLA, ABS and nylon 6 fabricated using fused deposition modeling and injection molding, *Composites Part B: Engineering*, 176 (2019) 107341.

[20] O. S. Carneiro, A. F. Silva, and R. Gomes, Fused deposition modeling with polypropylene, *Materials & Design*, 83 (2015) 768–776.

[21] NatureWorks, L., 2013. Ingeo biopolymer 4043D technical data sheet. URL: https://www.natureworksllc.com/~/media/Files/NatureWorks/Technical-Documents/Technical-Data-Sheets/TechnicalDataSheet_4043D_3D-monofilament_pdf.pdf.

[22] ASTM D3418-15 Standard test method for transition temperatures and enthalpies of fusion and crystallization of polymers by differential scanning calorimetry. West Conshohocken, PA: ASTM International; 2015.

[23] A. Rahimizadeh, J. Kalman, K. Fayazbakhsh, and L. Lessard, Recycling of fiberglass wind turbine blades into reinforced filaments for use in Additive Manufacturing, *Composites Part B: Engineering*, 175 (2019) 107101.

[24] ISO/ASTM 52921, Standard Terminology for Additive Manufacturing—Coordinate Systems and Test Methodologies, (2013), pp. 1–13.

[25] K. Fayazbakhsh, M. Movahedi, and J. Kalman, The impact of defects on tensile properties of 3D printed parts manufactured by fused filament fabrication, *Materials Today Communications*, 18 (2019) 140-148.

[26] ASTM D638-14, Standard Test Method for Tensile Properties of Plastics; ASTM International, (West Conshohocken, PA, USA).

[27] X. Zhou, S. J. Hsieh, and C.C. Ting, Modelling and estimation of tensile behaviour of polylactic acid parts manufactured by fused deposition modelling using finite element analysis and knowledge-based library, *Virtual and Physical Prototyping*, 13 (3) (2018) 177–190.

[28] B. Rankouhi, S. Javadpour, F. Delfanian, and T. Letcher, Failure Analysis and Mechanical Characterization of 3D Printed ABS With Respect to Layer Thickness and Orientation, *Journal of Failure Analysis and Prevention*, 16 (3) (2016) 467–481.

[29] S. Ahn, M. Montero, D. Odell, S. Roundy, and P.K. Wright, Anisotropic material properties of fused deposition modeling ABS, *Rapid prototyping journal*, 8 (4) (2002) 248–257.

Author information

Habiba Bougherara is a professor of the Department of Mechanical and Industrial Engineering, Ryerson University, Toronto, Canada. She received her Ph.D in Mechanical Engineering from École Polytechnique Montreal. Her research interests include advanced composite materials, modelling and mechanical characterization, biomaterials and biomechanics.